Microplastics and Nanoplastics

RESEARCH

Open Access

Use of metal-tagged environmentally representative micro- and nanoplastic particles to investigate transport and retention through porous media using single particle ICP-MS

Emily Lena Tran[1,2*], Shaun Bevers[1], Casey Smith[3], Stephanie Brown[3], Nathan Malone[3], D. Howard Fairbrother[3] and James F. Ranville[1]

Abstract

Microplastics and nanoplastics (collectively, MNPs) are increasingly entering soils, with potential adverse impacts to agriculture and groundwater. Environmental detection, characterization, and quantification of MNPs is difficult and subject to artifacts, often requiring labor-intensive separation from environmental matrices. These analytical challenges make it difficult to conduct experiments investigating specific MNP characteristics influencing their transport and fate, particularly when examining multiple plastic types at low concentrations. By synthesizing a suite of metal-tagged polymers, which are cryomilled to create polydisperse fragmented particle suspensions, single particle ICP-MS (spICP-MS) can be used to quantify MNP particle size and concentration in controlled fate and transport studies. Use of unique metal-polymer pairs enables accurate, simultaneous analysis of multiple MNP types which can be used to track total particle transport and retention within a variety of environmental matrices. This was demonstrated using saturated sand column transport experiments to quantify the movement of two plastics having different properties: tin-tagged polystyrene (Sn-PS) and tantalum-tagged polyvinylpyrrolidone (Ta-PVP). The behavior of these polydisperse, fragmented MNPs was compared to that of fluorescent, carboxylated monodisperse PS spherical microspheres (Fl-PS). Mobility of all MNP types increased with decreasing particle size, and hydrophilic Ta-PVP particles migrated more effectively than the hydrophobic Sn-PS particles. Furthermore, the addition of humic acid (HA) to the carrier solution increased the colloidal stability of both metal-tagged MNP suspensions, resulting in much greater elution from the column than in HA-free deionized water or moderately- hard water (ionic strength = 5mM). This combination of particle synthesis and spICP-MS analysis provides insights into the transport of MNP having physical properties that are representative of environmental MNPs and opens up a broad range of applications for study of MNP environmental fate and transport.

Keywords Column experiments, Particle size distribution, Colloid transport, Metal-tagged microplastics, spICP-MS

*Correspondence:
Emily Lena Tran
emilyt@gri.org.il
[1] Colorado School of Mines, Golden, CO 80401, USA
[2] Shamir Research Institute, 1290000 Katzrin, Israel
[3] Johns Hopkins University, Baltimore, MD 21218, USA

Introduction

A growing body of literature has been devoted to the fate and transport of microplastics and nanoplastics (MNPs) in terrestrial environments. It has been estimated that the global mass of plastics released to terrestrial environments is between 4–23 times greater than that released to the oceans

[1]. MNPs may enter agricultural soils through applications of MNP-containing fertilizers [2–4] and the use of plastic mulching films [5, 6]. In non-agricultural soils, MNPs may be found as a byproduct of tire erosion [7, 8], the disposal of plastic-containing wastewater [9] and the environmental decomposition of macro-plastic waste [10]. Understanding the fate and mobility of nanoplastics (NPs, < 1 μm) and microplastics (MPs, < 5 mm) in soils is of utmost importance, as MNPs have been shown to have toxicological impacts on soil and plant biota [11–14]. Additionally, mobile MNPs could facilitate transport of other secondary organic and inorganic contaminants, such as polymer additives or sorbed heavy metals, into the groundwater [15, 16]. Increasing concern has arisen regarding NPs [17, 18]. The majority of MP studies utilize optical microscopy to enumerate micron to millimeter-sized particles. This approach is not effective for sub-micron NP particles. This, in part, reflects the far fewer publications on NPs compared to MPs. Because NPs are often below the detection limits of mass-based or optical methods, and there is limited availability of environmentally-representative reference materials [19], far less is known about NP behavior in the environment as compared to MPs. However, their potential negative impact to the biosphere is much greater, as their small size enables them to move through cell membranes [20, 21].

Particle size is often a main parameter determining both subsurface mobility [22, 23] and ecotoxicity [24, 25]. Extrapolating from studies of particle transport in porous media, it is unlikely that environmentally-generated >10 μm MPs would penetrate the upper layer of soils [26]. While commercially available surface-modified, polystyrene microspheres have been often used to examine transport of MNPs of <10 μm, these are not representative of the polydisperse fragmented, and irregularly-shaped MNPs found in the environment [11, 27, 28]. Therefore, a need exists to develop techniques which can effectively examine the transport and fate of environmentally-relevant, polydisperse MNPs through porous media, which requires an ability to distinguish them from complex mineral and organic particle backgrounds. One option capable of reporting broad particle size distributions (PSDs) of irregularly-shaped particles is single particle inductively-coupled plasma- mass spectroscopy (spICP-MS), which has recently been used to characterize polydisperse suspensions of MPs directly based on their carbon content [29–31]. However, as the method in its current form does not allow for the measurement of particles below 1 μm, the use of this method still requires further optimization to be used to distinguish sub-micron sized particles from mainly carbon-based environmental matrices [32, 33].

Several recent studies have used metal-tagged plastics of a uniform, spherical nature as a method to track NPs through various organic matrices, allowing their distinction from the mainly carbon-based background [34–37]. However, most current metal-doped nanoplastics are monodisperse and spherical rather than polydisperse and fragmented, and their behavior may differ from more environmentally-representative particles whose PSD spans the nano- to micro range. Baalousha et al. [38] also recently developed a method to use the native elemental ratio fingerprint within plastic product waste to identify and characterize environmental, fragmented NPs, which may be an effective method for tracking environmentally-relevant particles in the future. However, thus far, the loading of the metals in "natural" microplastics is not fully known, and therefore this identification method has not yet been used in controlled transport studies.

Our study focuses on the transport properties of MNPs due to the clear need for improvement in their quantification, driven by their potential for environmental impact. Herein, we present results that demonstrate an improved analytical approach to investigate the behavior of environmentally representative MNPs, made possible by tagging plastic polymers with a metal additive uniformly dispersed within the polymer matrix [39, 40]. Examining transport by tracking a metal tag rather than the plastic polymer itself enables the use of the quantitative, element-specific technique of single particle inductively coupled plasma-mass spectrometry (spICP-MS). Similar metal-tagged MNPs have been used to investigate the fate of MNPs of homogenous size and shape, relying on standard ICP-MS for analysis of total particle mass [34, 36, 41]. This work builds on this concept and maintains the heterogeneity of the size distribution and morphology of the particles, allowing for the investigation of the transport properties of a more realistic particle population and enabling quantification by particle number and size distribution. Furthermore, in our method, labelling different plastic polymers with different metals enables multiple MNP types to be differentiated from one another in the same transport experiment.

This paper represents the first attempt at using spICP-MS to track the mobility of mixtures of metal-tagged, heterogeneous, irregularly-shaped MNPs through a column in a manner enabling both particle number counting and sizing against a complex background. The high sensitivity of the technique also enables quantification of deposited MNPs that are recovered from the column after completion of the transport experiments. This approach presents an alternative to microscopy-based counting and sizing techniques, with the benefit of measuring submicron sizes. Although other studies have either incorporated metal ions or metal nanoparticles into a polymer, or sorbed them to the MNP surface, these studies have invariably used MNPs of rather narrow size ranges and

uniform, generally spherical shape [34, 41, 42]. The broad continuous submicron size range of the MNPs used in this study enabled us to investigate the influence of size on mobility. This study intentionally focused on MNPs of size ranges <2 μm, as they are less likely to be retarded through filtration in column studies and field soils [26]; however, MNPs in this size range can be particular challenging to analyze as nano-scale appropriate techniques are at their upper limit and techniques used for larger MPs are at their lower limits of detection [32].

Methods and materials

MNP selection and preparation

Three types of particles were used in this study. Carboxylate-modified polystyrene fluorescent microspheres (Bangs Laboratories) were purchased in sizes of 0.1, 1.0 and 5.0 μm. Each size incorporates a different fluorophore with unique excitation and emission wavelengths such that their mass concentrations (μg/L) can be measured simultaneously in a fluorescence microplate reader (BioTek Synergy Neo2).

Two metal-tagged polymers, polyvinylpyrrolidone (PVP) and polystyrene (PS), were selected for use in transport experiments due to their different surface properties. PVP was chosen due to its hydrophilic nature, allowing it to remain stable in aqueous suspensions, and its environmental relevance given its use in pharmaceutical and foodstuff industries [43]. Polystyrene was chosen due to its ubiquitous use in consumer products and its hydrophobic properties that were expected to result in contrasting transport behavior as compared to PVP. The synthesis and characterization of the metal-doped MNPs has been extensively described in Smith et al. [40]. In short, a metal additive was dissolved at 1% mass concentration with the selected polymer in an organic solvent via sonication. The resulting plastic coupons were dried, cryomilled and filtered to achieve a powder of <35 μm. Organometallic complexes were selected based on their solubility in the same solvent used to dissolve the selected polymer, the metal's detection sensitivity, and its crustal abundance such that the polymer can be easily distinguished from soil and sediment backgrounds [40]. Metal homogeneity in the polymer was confirmed using μXRF [39, 40] as described in the supplementary material (SM, Figure S1). While Sn is known to be present in small quantities in the natural soils, the background of Sn observed in the background was consistently less than 1% of that observed in the Sn-PS suspension.

Of significance, the addition of these metal additives did not change the surface chemistry or surface properties of the MNPs, as evidenced by the lack of change in water contact angle measurements and XPS analysis conducted on plastics prepared both with and without the organometallic additives [40]. Furthermore, leaching of the metals was not observed over a period of 6 weeks [40]. Therefore, the final product produced is considered representative of environmentally-relevant MNPs.

MNP characterization

Surface properties

Zeta potential (Malvern ZetaSizer) was measured to determine particle surface charge prior to use in transport experiments. Measurements were performed in three separate solutions: deionized water (DI), a moderately hard synthetic freshwater (MHW) of ionic strength 5 mM, and a solution of 5 mg/L humic acid (HA, *Suwannee Stream Reference, USGS)* in MHW. The MHW was chosen as an electrolyte matrix which mimics environmental conditions. Its use and composition is described by the USEPA [44] and details are provided in the SM. The MHW-HA solution is the most representative of environmental conditions in which dissolved organic matter is present (particularly in soils) and therefore transport results from this set of conditions are emphasized.

Size distribution and morphology

Scanning electron microscope (SEM) images of the raw cryo-milled plastic powder were taken to qualitatively describe the morphology of the particles (details in SM). These images were solely used to determine the particle morphology and approximate the aspect ratio to determine if it was appropriate to use a spherical approximation to determine the equivalent particle sizes in subsequent analyses.

PSD of metal-tagged particle suspensions was measured using two separate methods. A single particle optical sizer (SPOS, PSS Nicomp Accusizer 770) was used to determine the broad PSD of particles in the 0.5–50 μm range. The PSD of the metal-tagged particles of 0.2–2.0 μm was quantified using spICP-MS (Perkin Elmer, Nexion 300D, further details below). The use of both instruments enabled the characterization of a broader size range of particles than either individual instrument is capable of measuring.

At the lower size range, spICP-MS was used to detect either ^{181}Ta or ^{118}Sn as appropriate. Specific details of spICP-MS parameters and sample introduction methods are detailed in the SM. Particle size was computed from the mass of metal detected in each MNP, the mass loading of the metal in the particle, and the particle density, assuming an equivalent spherical diameter and homogenous distribution of the metal tag in the polymer according to Eq. 1:

$$\text{Particle Volume (V)} = \text{Measured Pulse area} \times \frac{\text{Metal mass}}{\text{Pulse area}} \times \frac{\text{MP mass}}{\text{Metal mass}} \times \frac{1}{\text{MNP density}} \quad (1)$$

The effective particle diameter (d) can then be calculated according to Eq. 2:

$$V = \left(\frac{\pi d^3}{6}\right) \quad (2)$$

where V is the particle volume, and d is the particle diameter. The sum of the integration of the pulses yields the mass concentration (µg/ml).

The lower size limit measurable by the spICP-MS is established by the instrument sensitivity, the background signal, and the metal loading in the polymer as described in Bevers et al. [39]. The maximum particle size that can be efficiently transported and digested by the plasma for MNPs has been reported to be around 5 µm [30]. However, as particle size increases, the plasma is unable to fully ionize the particles, and transport efficiency into the plasma decreases, which effectively decreases the accuracy of particle number concentrations (PNCs) near the upper limits of the instrument [39]. Furthermore, given the power-law distribution of these particles in which the number of particles increases with decrease in particle size in an exponential relationship [39, 45], the number of particles in the upper (> 2.5 µm) size fraction is so low that the number of countable particles is not statistically significant upon correction for the dilution factor necessary to offset the effect of coincidence in the lower size ranges. Therefore, it was necessary to find a balance between measurable size range and particle "countability" in each size bin at the dilutions used in this study, and it was decided that the conservative estimate of the maximum size of particles to be enumerated should be 2 µm. Further discussion on the effect of dilution on implications for measuring transport can be found in the SM and Figure S5.

It is important to note that size distributions measured by both SPOS and spICP-MS are susceptible to coincidence as PNC increases. This phenomenon and its impacts are described in detail in the SM and in Bevers et al. 2023 [39]. In the context of column transport experiments, the issue of coincidence becomes particularly problematic as the particles change in concentration throughout each time step in the eluent, creating a possible source of error. Therefore, care was taken to dilute samples taken from each step in the experiment such that coincidence is minimized and particle concentrations in equivalent size bins can be normalized to a similar initial concentration.

Column experiments

A 25-cm long, vertically oriented glass HPLC column (diameter 0.63 cm) was modified for use in all particle transport experiments (Figure S2). Prior to every experiment, the column was wet-packed with washed sand that had been equilibrated overnight with the appropriate carrier solution. An HPLC pump was connected to the bottom to provide upward flow of degassed water at a flow rate of 0.15 ml/min. The pore volume of the column was calculated by the equation:

$$\varnothing * V = PV \quad (3)$$

where $\varnothing$ is the porosity of the sand (V/V, no units), V (cm^3) is the total volume of the glass column, and PV is the pore volume of the column (cm^3). The sand porosity, 0.42, was determined by measuring the weight of a known volume of dry and water-saturated sand and assuming that the sand particle density was 2.65 g/cm^3.

In each transport experiment, a single injection solution containing the Ta-PVP and Sn-PS MNPs, the fluorescent microspheres (0.1, 1.0, and 5.0 µm), and Br^- was prepared. The Br^- was employed as a non-reactive, conservative tracer to track the progress of all experiments. Injection solutions were analyzed by spICP-MS for ^{118}Sn and ^{181}Ta to obtain the initial particle PSD and PNCs. Particle mass concentrations injected into the column were ~ 50 mg/L for both Ta-PVP and Sn-PS. Similar concentrations of microplastics and nanoplastics have been detected in soils, particularly in agricultural fields in which plastic mulch is used or crops are irrigated with treated wastewater [46, 47]. However, the mass fraction of the particles detectable by the spICP-MS account for significantly less than this, as > 99% of the mass of the particles is accounted for by larger particles which are above the size detection limit of the instrument. Actual mass concentrations of detectable MNPs are in the range of µg/L, as might be present in the environment. The <2 µm fraction did contain the vast majority of the particle numbers present, consistent with other observations of a power-law relationship between size and number [39]. Fluorescent microsphere relative mass concentrations were measured using a fluorescence microplate reader (BioTek Synergy Neo2) against calibration curves prepared by diluting the injection solution. Particles were measured at excitation/emission wavelengths according to Table S1. ^{79}Br was measured by ICP-MS.

Transport experiments were conducted in replicate using deionized water, MHW, and MHW with 5 mg/L

HA (Table S2) according to the experimental protocol detailed in the SM. One PV of particle-containing solution was injected into the column at the commencement of each experiment, followed by 10 additional PVs of background solution wash. Samples were collected at the outlet using a fraction collector (ISCO Foxy 200) at 7-min increments until the experiment was concluded.

Sand was sampled from five locations along the length of the column for analysis of MNP deposition. Sand samples were collected using a small spatula to scrape sand into a pre-weighed test tube. Fractions were taken during the column cleaning process from the first several centimeters from the inlet (at 0–2, 2–4 and 4–6 cm, respectively), the middle of the column, and the last 2 cm prior to the exit of the column. Each fraction was dried until the weight remained stable, and the final weight of the dry sand was recorded. To each fraction, 5 mL of ultrapure water was added, and the sample was vortexed to release the MNPs retained by the sand. The sand was allowed to settle for ~ 1 min, and 1 mL of supernatant was immediately transferred to a new test tube. This fraction was then diluted to 5 mL using deionized water for spICP-MS analysis.

Analysis of transport

In each transport experiment, the concentration of particles eluted from the column over time was presented as a relative concentration to that injected into the column (C/C_0) and plotted as a factor of pore volumes eluted. Particle size data were binned into groups of 0.2–0.5 µm, 0.5–1.0 µm, 1.0–1.5 µm, and >1.5 µm, allowing for analysis of the influence of particle size on transport for particles of the same polymer type or the same size of different polymers. Alternatively, all of the particles can be summed together as a factor of either total PNC or total particle mass to compare overall mobility of MNPs of different polymer type. Total particle mass was calculated using the ICP element signal for each sample. Mass balance was calculated by subtracting the sum of the measured total mass of each bin for all samples collected at the outlet from the total injected mass of all particles in each size bin. Subsequently, deposition profiles of MNPs by location in the column were prepared to compare with size distributions of the eluted particles.

Attachment efficiency for particles of each size and polymer type was also calculated for particles in the HA and DI solutions by comparing the maximum C/C_0 reached at the peak of each breakthrough curve under unfavorable and favorable attachment conditions, as was described in [48]. In this case, MHW represents conditions favorable for attachment, while DI is less favorable and solutions containing HA are least favorable. Attachment α in a column experiment is defined by:

$$\alpha\eta_0 L = \frac{2d_c}{3(1-\varepsilon)} \bullet ln\frac{C}{C_0} \tag{4}$$

where η_0 is the collector efficiency of the immobile matrix (in this case sand), L is the length of the column, d_c is the collector diameter, ε is the column total porosity, and $\frac{C}{C_0}$ is the relative concentration of particles eluted from the column at a given time. When the experiment is carried out under favorable attachment conditions (in this case MHW), it can be assumed that the value of $\alpha = 1$, (i.e. every collision of particle and collector results in an attachment) [48]. Ultimately, the attachment coefficient under conditions unfavorable for attachment can be defined by:

$$\frac{ln\left(\frac{C}{C_0}\right)_{unfav}}{ln\left(\frac{C}{C_0}\right)_{fav}} = \alpha_{unfav} \tag{5}$$

where *unfav* and *fav* represent the maximum C/C_0 eluted under unfavorable and favorable conditions, respectively. This comparison approach eliminates many of the column-specific variables in Eq. 4, allowing for a reasonable approximation of α.

Results and discussion

Particle characterization

Particle morphology and size distribution

All metal-tagged particles showed a fragmented morphology in SEM images (SM Figure S3), due to the cryomilling process used to prepare them. This is representative of MNPs generated during natural environmental weathering processes. It was, however, determined that the aspect ratio of the particles is such that data generated by spICP-MS can be used to approximate a particle size and mass assuming a spherical morphology. This assumption is necessary in order to determine a particle size distribution for irregularly shaped particles if they are not rods or fibers [32].

The particle size distributions for all metal-tagged particles in the 0.5–10 µm range measured by SPOS and in the 0.2–2.0 µm range measured by spICP-MS in a representative injection solution (MHW with 5 mg/L HA) are shown in Fig. 1. While SPOS does measure a larger range of particle sizes than spICP-MS, it is limited by its large lower size limit and its inability to distinguish between particle types. For data from both instruments, the measured number-based size distribution was converted to a normalized mass-based size distribution assuming a spherical morphology, which was then normalized to the sum of the total mass. As observed in SPOS data (Fig. 1A), much of the mass of both particle types lies in the larger particle sizes (>2 µm). However,

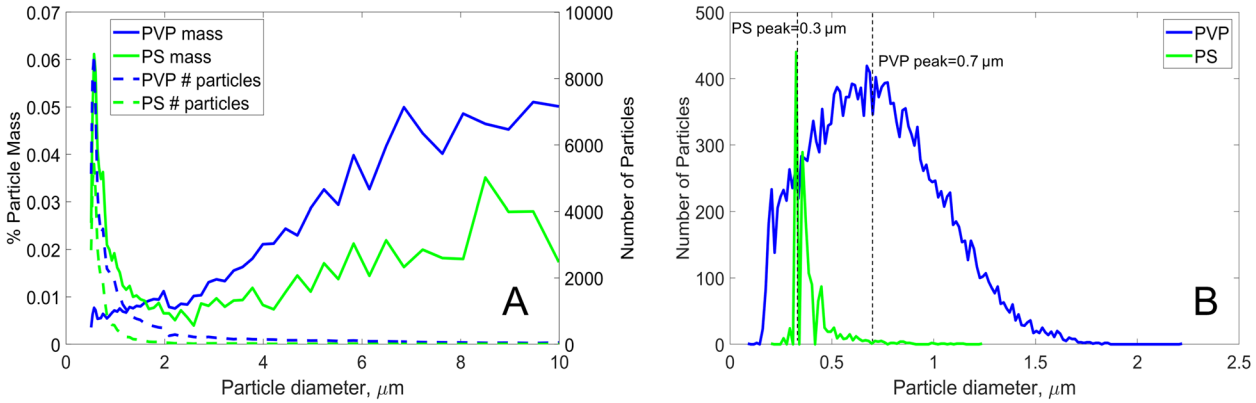

Fig. 1 Size distribution of PVP and PS MPs in MHW with 5 mg/L HA, as measured by both (**A**) SPOS, showing the distribution as a function of particle number (dotted lines) and mass (solid lines) of particles from 0.5–10 µm and by (**B**) spICP-MS, demonstrating the size distribution of particles in the 0.2–2.0 µm range

the vast majority of Ta-PVP and Sn-PS particles are <2 µm diameter, which is compatible with the size range that can be reliably measured by the spICP-MS as previously described. In the <2 µm range, the SPOS and spICP-MS data qualitatively agree, showing that most of the measurable Sn-PS particles are in the smaller size range, while a greater proportion of PVP particles are distributed between 0.2–1.5 µm. This size distribution agrees with that reported for similar particles by Bevers et al. [39] showing that nearly all Ta-PVP particles fall into the <2 µm range. However, Bevers et al. [39] also notes that the PSD is highly dilution-dependent. Our data follows this trend, as shown in Figure S5 in which a 10-fold dilution significantly shifted the PSD to smaller particle sizes. In particle size measurements by spICP-MS (Fig. 1B), Ta-PVP particles appear to exhibit a normal distribution with a peak near 0.7 µm. However, this apparent PSD only represents that at a single dilution. At a similar mass concentration of 50 mg/L, there is a scarcity of Sn-PS particles in this size range. The SPOS data (Fig. 1A) also show relatively low numbers (5640 particles) of Sn-PS in the 1–4 µm range as compared to PVP (13996 particles). Taken together, these data indicate that the total number of spICP-MS measurable Sn-PS particles was lower than that of the Ta-PVP particles.

Zeta potential

Zeta potential was dependent on both the particle type and the water matrix in which the particles were suspended. In deionized water, the zeta potential of Sn-PS and Ta-PVP particles was found to be roughly the same (-11 and -14 mV, respectively (Figure S4)). Carboxylate-modified fluorescent PS microspheres (Fl-PS) were much more negative, at approximately -30 mV. The zeta potential of particles in MHW was not significantly different than that in DI (-13, -15 and -30 for PVP, PS and Fl-PS, respectively). The addition of HA to MHW resulted in more negative surface charges for the Ta-PVP and Sn-PS MNPs of -17 and -27, respectively. Natural organic matter coatings have been shown to impart a more negative charge onto suspended particles [49–51]. The highly negatively charged surface of the carboxylated Fl-PS was not significantly impacted by the adsorption of HA, likely because the negative charge introduced by the abundance of carboxyl groups limited the degree to which adsorbed HA could modify the already high negative surface charge. For the MNPs, the impact of ionic strength and addition of HA on the particle zeta potentials was greater for the Sn-PS particles than for the Ta-PVP particles. Because of the greater hydrophobicity of the Sn-PS surface, hydrophobic interactions likely lead to greater sorption of HA, resulting in a larger change in zeta potential [52].

Column experiments

Tracer breakthrough

Differences in sand packing resulted in minor variation in Br^- transport behavior between experiments, as seen by the Br breakthroughs (Figure S6). In all experiments, Br^- appeared to break through around 0.5 PV. Hydrodynamic dispersion during transport through the column resulted in a maximum C/C_0 ranging from 0.8 to nearly 1. Our unique metal-polymer combinations and use of multiple fluorophores in the PS microspheres enabled simultaneous measurements of transport behavior of mixtures of Ta-PVP, Sn-PS and Fl-PS in each experiment. Thus, comparisons between different particle types and sizes are not subject to differences in water flow between experiments. Additionally, bromide results suggest the experiments are hydrologically comparable for the purpose of

observing the impact of the carrier solution and polymer chemistry on particle transport.

Microsphere transport

Figure 2A shows breakthrough curves from a representative experiment demonstrating the size-dependence of the Fl-PS on particle mobility. Early elution of the particles compared to bromide suggest a minor degree of size exclusion, a phenomena commonly observed for colloid transport [53]. The maximum C/C_0 of each of the 0.1, 1.0 and 5.0 µm Fl-PS particles were 0.64, 0.44 and 0.12, respectively, and the corresponding recoveries for each size fraction was 86%, 58% and 14%, respectively. Together, these data indicate that larger particles were retained in the column to a greater extent than smaller ones.

Similar recoveries and trends have been reported in a sand column using negatively charged fluorescent microspheres of 0.2 and 1.0 µm [54]. The authors attributed the retention in part to straining, as it has been reported that straining is a dominant retention mechanism when the particle to sand-grain diameter ratio is greater than 0.008 [55]. This was the case for the 5 µm particles in our sand which was sieved to use only the 250–500 µm fraction. Below this size, it is likely that particles were mainly affected by physiochemical deposition.

The chemical composition of the carrier fluid also influenced the mobility of the particles. In comparison to its recovery of 58% in HA, the 1.0 µm Fl-PS exhibited a recovery of 52% in DI and only 18% in MHW. The corresponding maximum C/C_0 of 1.0 µm Fl-PS in HA, DI and MHW was 0.44, 0.22 and 0.04, respectively, as can be observed in Fig. 2B. Increasing ionic strength is known to correlate with decreasing particle mobility, resulting from increasing aggregation and deposition rates [56]. The higher Fl-PS elution in the presence of HA was consistent with other studies of PS transport [49, 51], which demonstrated that carboxylated PS spherical microspheres are most mobile in the presence of dissolved organic matter. As both the ionic strength and presence of HA appeared to minimally affect the zeta potential of the FL-PS microspheres, the differences in mobility are more likely a result of (a) modification of the surface of the sand grains, or (b) in the case of HA, an additional steric stabilization of the Fl-PS microspheres. This latter process could also explain the lack of loss 0.1 µm Fl-PS by particle attachment in the HA experiments.

Mobility of Ta-PVP

Figure 3A demonstrates the mobility of a Ta-PVP suspension in a single experiment as a factor of particle size using bins of 0.2–0.5 µm, 0.5–1.0 µm, 1.0–1.5 µm, and > 1.5 µm. Particles <0.2 µm may have been present but were below the size quantifiable by spICP-MS under the given study conditions, as previously described in Sect. 2.2.2. Similar to the behavior of the fluorescent microspheres, Ta-PVP particles of smaller sizes migrated through the column more efficiently than those of larger sizes (Fig. 3A). Percent recovery by particle number for particle size bins of 0.2–0.5 µm, 0.5–1.0 µm, 1.0–1.5 µm, and >1.5 µm in the presence of 5 mg/L HA were 54%, 22%, 11%, and 3.7%, respectively. These recoveries agree with the corresponding calculated attachment efficiencies for particles in each these bins, which were calculated by Eq. 5 to be 0.24, 0.35 and 0.47, respectively. The inverse relationship of Ta-PVP particle size with mass recovery was consistent throughout all experiments performed, regardless of carrier solution chemistry. Several studies have also demonstrated the size dependence of α in which increasing particle size results in increases in α [50, 57].

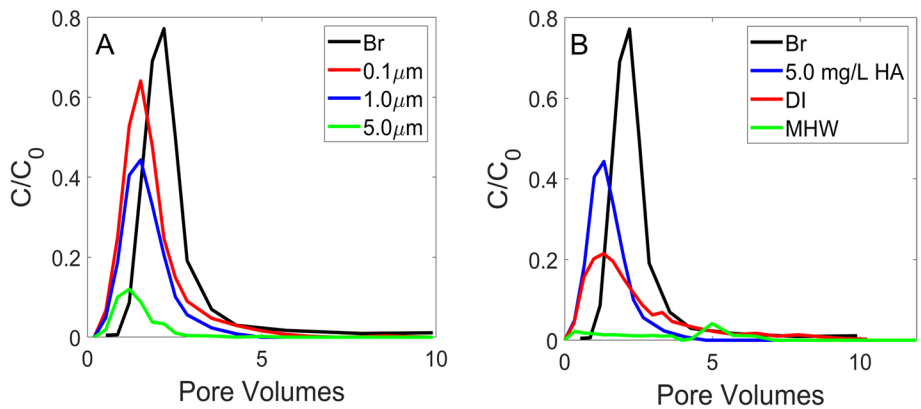

Fig. 2 Mobility of fluorescent microspheres (**A**) in the presence of humic acid (5 mg/L) as a factor of size, and (**B**) breakthrough curves of 1.0 µm fluorescent microspheres through sand in HA, DI and MHW carrier solutions, with representative Br breakthrough curve

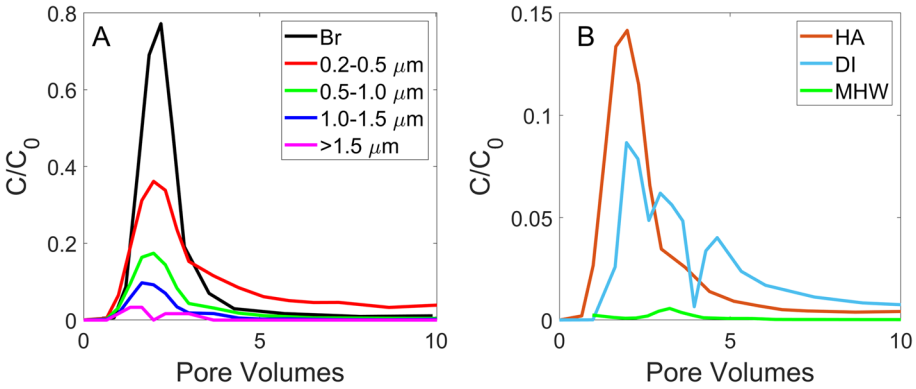

Fig. 3 Breakthrough of PVP particles in the presence of (**A**) 5 mg/L humic acid, binned into 0.2–0.5, 0.5–1.0, 1.0–1.5 μm and >1.5 μm size ranges and (**B**) total particle mass in different carrier solutions

Generally, few particles measured in the effluent were >1.5 μm, although it must be cautioned that the upper size limit of spICP-MS for quantification of microplastics is approximately 2 μm, as described in Sect. 2.2.2. The breakthrough curve for >1.5 μm is shown in Fig. 3A, but is presented only qualitatively for reference.

Figure 3B shows the overall mobility by relative mass of the entire Ta-PVP suspension as a factor of carrier solution chemistry. Note that the maximum C/C_0 attained as a factor of total particle mass in HA ($C/C_0 \sim 0.15$) is approximately an average of the maximum C/C_0 reached for each particle size bin in Fig. 3A ($C/C_o = 0.05–0.35$), showing that this total breakthrough curve is a composite of the various particle size fractions in the same suspension. This maximum C/C_0 will be more heavily weighted towards the size bin in which most particle mass is present; in this case, 1.0–1.5 μm.

The impact of surface chemistry on the mobility of the Ta-PVP particles was similar to that of the fluorescent microspheres in that the greatest maximum C/C_0 (0.14) was observed in the presence of HA, and the lowest maximum C/C_0 (0.006) was observed in MHW. It has been well-documented that particle transport efficiency decreases with increasing ionic strength [48, 50, 58] due to the compression of the double layer leading to increased attachment and deposition of particles. More importantly, HA and other natural organic matter masks the impact of ionic strength on transport by coating the particles and increasing repulsive surface charge, resulting in increased transport efficiency. Additional studies have also shown that HA, in particular, has a dominant impact on measured α of particles to collector surfaces [48–50]. Geitner et al. [48], for instance, reported decreasing α for PVP-functionalized Ag particles with increasing HA concentration through glass microspheres and kaolinite using both column and batch experiments. In contrast to the Fl-PS, where HA did not change the zeta potential, surface charge was greater for Ta-PVP in HA/MHR versus MHR only solutions. Electrosteric stabilization may thus play a greater role for increased mobility of Ta-PVP.

Mobility of different polymers

In Fig. 4A, transport of total Ta-PVP and Sn-PS can be observed simultaneously, with the relative mobility of the 1.0 μm Fl-PS shown for reference. It should be noted that the particle size distribution for each injected stock MNP suspension was different (Fig. 1B), which accounts for some of the differences in total mass transport between particle types. However, the α for Sn-PS particles in the 0.2–0.5 μm size range was 0.9, which corresponded to a mass recovery of 29%, in comparison to the calculated α of 0.24 for the Ta-PVP particles (mass recovery = 54%) under similar chemical conditions in the same particle size bin. Too few Sn-PS particles were eluted in other larger size bins to yield robust α and recovery calculations.

In nearly all cases, the fluorescent microspheres reached a much greater C/C_0 and exhibited higher recoveries than either of the metal-labelled MNPs. This is partially due to their carboxylated surface, leading to a lower zeta potential (~-30 under all conditions) and more stable nature. It is also due to their perfectly spherical shape, which has been shown to be more mobile through porous media than non-spherical shapes such as fragments and fibers [59, 60]. In Fig. 4B, an example is given in which similarly sized carboxylated beads reach a much greater maximum C/C_0 (0.64) than the most mobile size fractions of either the Ta-PVP and Sn-PS under similar chemical conditions.

In the absence of HA, Sn-PS was mostly not observed in the eluent, partially due to the low concentration of initial particle numbers and partially due to their unstable

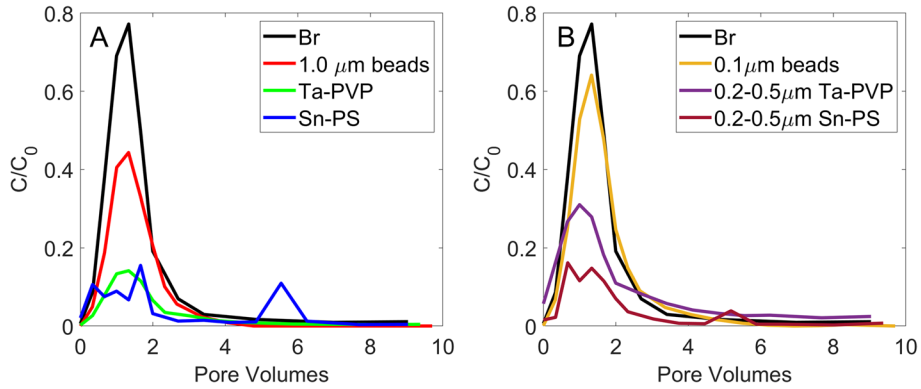

Fig. 4 Breakthrough of PVP and PS particles in the presence of 5 mg/L humic acid. (**A**) All particles measured by spICP-MS as a function of total mass in comparison to 1.0 μm fluorescent microspheres and conservative tracer, Br. (**B**) Breakthrough for particles detected in the 0.2–0.5 μm size bin in comparison to the 0.1 μm fluorescent microspheres

nature. However, in the presence of HA, quantifiable breakthrough of Sn-PS was observed, as organic matter coated and stabilized the particles. This is supported by the substantial drop in zeta potential from -15 to -27 mV in the absence and presence of HA, respectively. In experiments with HA, a spiky and uneven breakthrough pattern was observed for Sn-PS, attributable to the small initial particle number injected into the column. Similar transport behavior of pristine PS where MPs were eluted in short, discreet, high concentration spikes was reported by Shaniv et al. [51]. However, few studies have been conducted on polydisperse, irregularly shaped PS particle suspensions such as those employed here. These results suggest that hydrophobic plastics in soil solutions containing high concentrations of natural organic matter, such as in agricultural soils, would be highly mobile and potentially infiltrate deep into the soil.

To better control for differences in particle size distribution between particle types, transport of different polymers in equivalent size bins can also be compared. Figure 4B shows the breakthrough of the 0.1 μm fluorescent microspheres in comparison to the Ta-PVP and Sn-PS particles that were bracketed into similar size ranges (0.2–0.5 μm) to demonstrate the differences in transport behavior due to polymer type and surface properties and neglect the influence of particle size. Both Ta-PVP and Sn-PS were less mobile than the Fl-PS in all cases. Despite the increased zeta potential imparted to the Ta-PVP and Sn-PS by the HA coating (-17 and -26 mV, respectively), the Fl-PS exhibited a greater zeta potential (-30 mV) as a result of its carboxylated surface. Furthermore, the metal-modified MNP are heterogeneous, irregularly shaped fragments more typical of environmentally relevant MNPs than engineered microspheres, which may be more retarded in transport than spherical particles of similar composition and shape as previously discussed.

Deposition of particles in column

The high sensitivity of spICP-MS with respect to particle number facilitates detection of small quantities of particles retained within the sand matrix, on the order of a few tenths of a ng of MNP per gram of sand. Figure 5 presents the deposition of Ta-PVP and Sn-PS particles along the column in the experiment with HA in the carrier solution. The mass of each polymer was summed for all particles measured in each size bin, and the data were presented as total mass of particles in each size bin normalized to the weight of the dry sand sample. In all experiments performed, most of the Ta-PVP was deposited close to the inlet of the column (0–6 cm), and very few Ta-PVP particles were detected near the exit of the column. Particles detected near the exit of the column were nearly always in the smallest (0.2–0.5 μm) size fraction, consistent with their greater overall mobility of smaller sizes, which undergo less filtration. No particles in the largest (>1.5 μm) size fraction were detected at the end of the column.

Sn-PS were deposited later in the column, albeit in larger particle sizes (Fig. 5B). It appeared many larger particles (>1.5 μm) were deposited in the sand near the end of the column in comparison to that which was injected into the column (see PSD in Fig. 1B). This could be due to the hydrophobic particles being captured by a small amount of trapped air that may have accumulated near the top of the column. Though experiments were all assumed to be saturated, the presence of a small amount of air introduced into the column could possibly trap hydrophobic colloids such as PS particles at the air–water interface [61–63], leading to high concentrations of particles. If these particles are then released together, coincidence would then lead to the apparent presence of very large particles in analysis. Hydrophilic colloids such as the Ta-PVP would be less affected by a small amount of trapped air, as they tend to be repelled from air–water

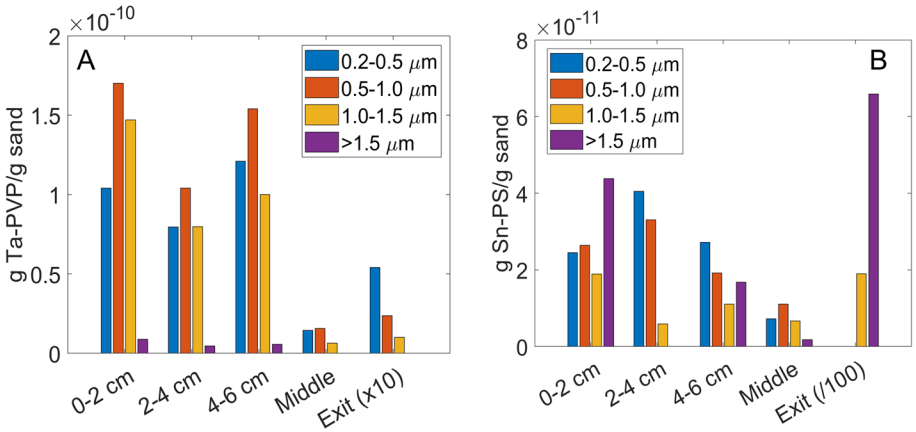

Fig. 5 Deposition of particles at different locations along the sand column length. (**A**) and (**B**) show binned particle sizes of Ta-PVP and Sn-PS along the column length, respectively. Mass is normalized to the mass of the sand sample taken from the column. Note that the "Exit" location for PVP represents 10 × the measured sizes and the "Exit" location for PS represents 1/100 of the measured sizes, for comparison to the other locations

interfaces which may have similar negative charges to the colloid surface [62].

Conclusions

This work demonstrates that spICP-MS analysis of polydisperse metal-tagged MNPs is an effective technique to conduct research on transport of environmentally representative concentrations of a variety of plastic types at the sub-micron scale. Both Ta-PVP and Sn-PS particles could be simultaneously detected in eluent from a saturated sand column and characterized by particle size and concentration, eliminating experiment comparison errors due to differences in column packing and resulting hydrological parameters. Furthermore, in each experiment, particles of both polymer types could be detected and characterized along the column length to determine deposition behaviors. It was shown that Ta-PVP particles were generally more mobile than Sn-PS, as both maximum relative concentrations and total particle recoveries were greater for Ta-PVP than for Sn-PS particles in similar size bins. However, the low number of particles recovered in the eluent for Sn-PS and Ta-PVP in MHW resulted in sometimes low statistical robustness. In these cases, particle transport could be compared as a factor of total particle mass, which was measured by total resolved intensity of each metal tag in each sample. In all cases, the greatest recovery of all particles investigated (Fl-PS, Ta-PVP and Sn-PS) was observed in the presence of 5 mg/L humic acid, which served to stabilize the particles.

This technique can be used to shed light on the influence of particle size and polymer type on plastic particle transport at the micro- and nano-scale that, to-date, has been difficult to investigate using current analytical techniques. Future research using this approach may include further investigation of the influence of particle irregularity in shape (fragment vs. sphere) by increasing resolution of sampling to better evaluate physical processes, changing the concentrations of particles used in injection solutions, changing the choice of metal tags based on the porous matrix chosen, and using various other chemical compositions of carriers fluids. The technique has great potential to compare the mobility of plastic particles composed of different polymer types simultaneously at environmentally representative concentrations. As the technique uses metals that are generally absent in background matrices, this can also be used to determine deposition profiles of plastics without the need to perform complex separation techniques. Together, these advantages yield the ability to conduct more environmentally representative research on plastic particle transport in porous media using a high-throughput and cost-effective sample analysis method.

Abbreviations

DI	Deionized Water
Fl-PS	Fluorescent-labelled polystyrene
HA	Humic Acid
HPLC	High Pressure Liquid Chromatography
ICP-MS	Inductively-coupled plasma mass spectrometer
MHW	Modified Hard Water
MNPs	Micro- and Nano-plastics
MPs	Microplastics
NPs	Nanoplastics
PNC	Particle Number Concentration
PS	Polystyrene
PSD	Particle size distribution
PV	Pore Volume
PVP	Polyvinylpyrrolidone
SEM	Scanning electron microscope
Sn-PS	Tin-labelled polystyrene
spICP-MS	Single particle inductively-coupled plasma mass spectrometer
SPOS	Single particle optical sensing
Ta-PVP	Tantalum-labelled polyvinylpyrrolidone

Supplementary Information

The online version contains supplementary material available at https://doi.org/10.1186/s43591-024-00087-5.

Supplementary Material 1.

Acknowledgements
The authors are grateful to Dr. Katha Pfaff at the CSM Minerals and Materials Characterization Facility for XRF and SEM analyses.

Authors' contributions
ELT performed column experiments and prepared the manuscript. SB assisted with spICP-MS analysis and provided scientific insight. DHF and JFR acquired funding and provided oversight and guidance. CS, SB and NM prepared the tagged plastic particles used in this study. All authors approved the final version of the manuscript.

Funding
The authors would like to acknowledge partial support from NSF-ECS 2003400.

Availability of data and materials
The datasets used and/or analyzed during the current study are available from the corresponding author on reasonable request.

Declarations

Ethics approval and consent to participate
Not applicable.

Consent for publication
Not applicable.

Competing interests
The authors declare no competing interests.

Received: 2 January 2024 Accepted: 2 May 2024
Published online: 14 May 2024

References

1. Horton AA, Walton A, Spurgeon DJ, Lahive E, Svendsen C. Microplastics in freshwater and terrestrial environments: Evaluating the current understanding to identify the knowledge gaps and future research priorities. Sci Total Environ. 2017;586:127–41.
2. Piehl S, Leibner A, Löder MGJ, Dris R, Bogner C, Laforsch C. Identification and quantification of macro- and microplastics on an agricultural farmland. Sci Rep. 2018;8(1):1–9.
3. Nizzetto L, Futter M, Langaas S. Are agricultural soils dumps for microplastics of urban origin? Environ Sci Technol. 2016;50(20):10777–9.
4. van den Berg P, Huerta-Lwanga E, Corradini F, Geissen V. Sewage sludge application as a vehicle for microplastics in eastern Spanish agricultural soils. Environ Pollut. 2020;261:114198.
5. Ramos L, Berenstein G, Hughes EA, Zalts A, Montserrat JM. Polyethylene film incorporation into the horticultural soil of small periurban production units in Argentina. Sci Total Environ. 2015;523:74–81.
6. Steinmetz Z, Wollmann C, Schaefer M, Buchmann C, David J, Tröger J, et al. Plastic mulching in agriculture. Trading short-term agronomic benefits for long-term soil degradation? Sci Total Environ. 2016;550:690–705.
7. Jan Kole P, Löhr AJ, Van Belleghem FGAJ, Ragas AMJ. Wear and tear of tyres: a stealthy source of microplastics in the environment. Int J Environ Res Public Health. 2017;14(10):1265.
8. Wagner S, Klöckner P, Reemtsma T. Aging of tire and road wear particles in terrestrial and freshwater environments–a review on processes, testing, analysis and impact. Chemosphere. 2022;288:132467.
9. Gündoğdu S, Çevik C, Güzel E, Kilercioğlu S. Microplastics in municipal wastewater treatment plants in Turkey: a comparison of the influent and secondary effluent concentrations. Environ Monit Assess. 2018;190(11):1–10.
10. Chae Y, An YJ. Current research trends on plastic pollution and ecological impacts on the soil ecosystem: a review. Environ Pollut. 2018;240:387–95.
11. Rozman U, Turk T, Skalar T, Zupančič M, Čelan Korošin N, Marinšek M, et al. An extensive characterization of various environmentally relevant microplastics – Material properties, leaching and ecotoxicity testing. Sci Total Environ. 2021;773:145576.
12. Guo JJ, Huang XP, Xiang L, Wang YZ, Li YW, Li H, et al. Source, migration and toxicology of microplastics in soil. Environ Int. 2020;137:105263.
13. Ng ELL, Huerta Lwanga E, Eldridge SM, Johnston P, Hu HWW, Geissen V, et al. An overview of microplastic and nanoplastic pollution in agroecosystems. Sci Total Environ. 2018;627:1377–88.
14. Zhou P, Wang L, Gao J, Jiang Y, Adeel M, Hou D. Nanoplastic–plant interaction and implications for soil health. Soil Use Manag. 2023;39(1):13–42.
15. Viaroli S, Lancia M, Re V. Microplastics contamination of groundwater: current evidence and future perspectives. A review. Sci Total Environ. 2022;824:153851.
16. Ren Z, Gui X, Xu X, Zhao L, Qiu H, Cao X. Microplastics in the soil-groundwater environment: aging, migration, and co-transport of contaminants – A critical review. J Hazard Mater. 2021;419:126455.
17. Hartmann NB, Hüffer T, Thompson RC, Hassellöv M, Verschoor A, Daugaard AE, et al. Are we speaking the same language? Recommendations for a definition and categorization framework for plastic debris. Environ Sci Technol. 2019;53(3):1039–47.
18. Gigault J, ter Halle A, Baudrimont M, Pascal PY, Gauffre F, Phi TL, et al. Current opinion: what is a nanoplastic? Environ Pollut. 2018;235:1030–4.
19. Ivleva NP. Chemical analysis of microplastics and nanoplastics: challenges, advanced methods, and perspectives. Chem Rev. 2021;121(19):11886–936.
20. Mitrano DM, Wick P, Nowack B. Placing nanoplastics in the context of global plastic pollution. Nat Nanotechnol. 2021;16(5):491–500.
21. Shen M, Zhang Y, Zhu Y, Song B, Zeng G, Hu D, et al. Recent advances in toxicological research of nanoplastics in the environment: a review. Environ Pollut. 2019;252:511–21.
22. Rillig MC, Ziersch L, Hempel S. Microplastic transport in soil by earthworms. Sci Rep. 2017;7(1):1–6.
23. O'Connor D, Pan S, Shen Z, Song Y, Jin Y, Wu WM, et al. Microplastics undergo accelerated vertical migration in sand soil due to small size and wet-dry cycles. Environ Pollut. 2019;249:527–34.
24. Lambert S, Scherer C, Wagner M. Ecotoxicity testing of microplastics: Considering the heterogeneity of physicochemical properties. Integr Environ Assess Manag. 2017;13(3):470–5.
25. Kim SW, Kim D, Jeong SW, An YJ. Size-dependent effects of polystyrene plastic particles on the nematode Caenorhabditis elegans as related to soil physicochemical properties. Environ Pollut. 2020;258:113740.
26. Yu Y, Flury M. Current understanding of subsurface transport of micro- and nanoplastics in soil. Vadose Zone J. 2021;20(2):e20108.
27. Rozman U, Kalčikova G. Seeking for a perfect (non-spherical) microplastic particle – The most comprehensive review on microplastic laboratory research. J Hazard Mater. 2022;424:127529.
28. Wong JKH, Lee KK, Tang KHD, Yap PS. Microplastics in the freshwater and terrestrial environments: Prevalence, fates, impacts and sustainable solutions. Sci Total Environ. 2020;719:137512.
29. Bolea-Fernandez E, Rua-Ibarz A, Velimirovic M, Tirez K, Vanhaecke F. Detection of microplastics using inductively coupled plasma-mass spectrometry (ICP-MS) operated in single-event mode. J Anal At Spectrom. 2020;35(3):455–60.
30. Laborda F, Trujillo C, Lobinski R. Analysis of microplastics in consumer products by single particle-inductively coupled plasma mass spectrometry using the carbon-13 isotope. Talanta. 2021;221:121486.
31. Hendriks L, Mitrano DM. Direct measurement of microplastics by carbon detection via single particle ICP-TOFMS in complex aqueous suspensions. Environ Sci Technol. 2023;57(18):7263–72.
32. Caputo F, Vogel R, Savage J, Vella G, Law A, Della Camera G, et al. Measuring particle size distribution and mass concentration of nanoplastics and microplastics: addressing some analytical challenges in the sub-micron size range. J Colloid Interface Sci. 2021;588:401–17.

33. Lusher AL, Bråte ILN, Munno K, Welden NA, Hurley RR. Is It or Isn't It: the importance of visual classification in microplastic characterization. Appl Spectroscopy. 2020;74(9):1139–53.
34. Keller AS, Jimenez-Martinez J, Mitrano DM. Transport of nano- and microplastic through unsaturated porous media from sewage sludge application. Environ Sci Technol. 2020;54(2):911–20.
35. Harycki S, Gundlach-Graham A. Single-particle ICP-TOFMS with online microdroplet calibration: a versatile approach for accurate quantification of nanoparticles, submicron particles, and microplastics in seawater. Anal Chem. 2023;95(41):15318–24.
36. Redondo-Hasselerharm PE, Vink G, Mitrano DM, Koelmans AA. Metal-doping of nanoplastics enables accurate assessment of uptake and effects on Gammarus pulex. Environ Sci Nano. 2021;8(6):1761–70.
37. Marigliano L, Grassl B, Szpunar J, Reynaud S, Jiménez-Lamana J. Nanoplastic labelling with metal probes: analytical strategies for their sensitive detection and quantification by ICP mass spectrometry. Molecules. 2021;26(23):7093.
38. Baalousha M, Wang J, Nabi MM, Alam M, Erfani M, Gigault J, et al. The elemental fingerprint as a potential tool for tracking the fate of real-life model nanoplastics generated from plastic consumer products in environmental systems. Environ Sci: Nano. 2024;11(1):373–88.
39. Bevers SG, Smith C, Brown S, Malone N, Fairbrother DH, Goodman AJ, et al. Improved methodology for the analysis of polydisperse engineered and natural colloids by single particle inductively coupled plasma mass spectrometry (splCP-MS). Environ Sci: Nano. 2023;10(11):3136–48.
40. Smith C, Brown S, Malone N, Bevers S, Ranville J, Fairbrother DH. Nanoplastics prepared with uniformly distributed metal-tags: a novel approach to quantify size distribution and particle number concentration of polydisperse nanoplastics by single particle ICP-MS. Environ Sci.: Nano. 2023;11:911–23.
41. Tophinke AH, Joshi A, Baier U, Hufenus R, Mitrano DM. Systematic development of extraction methods for quantitative microplastics analysis in soils using metal-doped plastics. Environ Pollut. 2022;311:119933.
42. Lai Y, Dong L, Li Q, Li P, Hao Z, Yu S, et al. Counting nanoplastics in environmental waters by single particle inductively coupled plasma mass spectroscopy after cloud-point extraction and in situ labeling of gold nanoparticles. Environ Sci Technol. 2021;55(8):4783–91.
43. Julinová M, Kupec J, Houser J, Slavík R, Marušincová H, Lenkačerveňáková LL, et al. Removal of polyvinylpyrrolidone from wastewater using different methods. Water Environ Res. 2012;84(12):2123–32.
44. Webber CI. Methods for measuring the acute toxicity of effluents and receiving waters to freshwater and marine organisms. Washington D.C.: Environmental Monitoring Systems Laboratory, Office of Research and Development, US Environmental Protection Agency; 1991.
45. Goodman AJ, Ranville JF. Single particle inductively coupled plasma mass spectrometry: a new method to detect geochemical anomalies in stream sediments. J Geochem Explor. 2023;251:107231.
46. Li W, Wufuer R, Duo J, Wang S, Luo Y, Zhang D, et al. Microplastics in agricultural soils: Extraction and characterization after different periods of polythene film mulching in an arid region. Sci Total Environ. 2020;749:141420.
47. Yu L, Zhang JD, Liu Y, Chen LY, Tao S, Liu WX. Distribution characteristics of microplastics in agricultural soils from the largest vegetable production base in China. Sci Total Environ. 2021;756:143860.
48. Geitner NK, O'Brien NJ, Turner AA, Cummins EJ, Wiesner MR. Measuring nanoparticle attachment efficiency in complex systems. Environ Sci Technol. 2017;51(22):13288–94.
49. Franchi A, O'Melia CR. Effects of natural organic matter and solution chemistry on the deposition and reentrainment of colloids in porous media. Environ Sci Technol. 2003;37(6):1122–9.
50. Pelley AJ, Tufenkji N. Effect of particle size and natural organic matter on the migration of nano- and microscale latex particles in saturated porous media. J Colloid Interface Sci. 2008;321(1):74–83.
51. Shaniv D, Dror I, Berkowitz B. Effects of particle size and surface chemistry on plastic nanoparticle transport in saturated natural porous media. Chemosphere. 2021;262:127854.
52. Song Y, Zhao J, Zheng L, Zhu W, Xue X, Yu Y, et al. Adsorption behaviors and mechanisms of humic acid on virgin and aging microplastics. J Mol Liq. 2022;363:119819.
53. Sirivithayapakorn S, Keller A. Transport of colloids in saturated porous media: a pore-scale observation of the size exclusion effect and colloid acceleration. Water Resour Res. 2003;39(4):1109.
54. Shani C, Weisbrod N, Yakirevich A. Colloid transport through saturated sand columns: Influence of physical and chemical surface properties on deposition. Colloids Surf, A. 2008;316(1):142–50.
55. Xu S, Gao B, Saiers JE. Straining of colloidal particles in saturated porous media. Water Resour Res. 2006; 42(12).
56. Petosa AR, Jaisi DP, Quevedo IR, Elimelech M, Tufenkji N. Aggregation and deposition of engineered nanomaterials in aquatic environments: Role of physicochemical interactions. Environ Sci Technol. 2010;44(17):6532–49.
57. Shen C, Huang Y, Li B, Jin Y. Predicting attachment efficiency of colloid deposition under unfavorable attachment conditions. Water Resour Res. 2010;46(11):11526.
58. Bennacer L, Ahfir ND, Alem A, Wang H. Coupled effects of ionic strength, particle size, and flow velocity on transport and deposition of suspended particles in saturated porous media. Transp Porous Media. 2017;118(2):251–69.
59. Seymour MB, Chen G, Su C, Li Y. Transport and retention of colloids in porous media: does shape really matter? Environ Sci Technol. 2013;47(15):8391–8.
60. Waldschläger K, Schüttrumpf H. Infiltration behavior of microplastic particles with different densities, sizes, and shapes-from glass spheres to natural sediments. Environ Sci Technol. 2020;54(15):9366–73.
61. Wan J, Wilson JL. Colloid transport in unsaturated porous media. Water Resour Res. 1994;30(4):857–64.
62. Flury M, Aramrak S. Role of air-water interfaces in colloid transport in porous media: a review. Water Resour Res. 2017;53(7):5247–75.
63. Norrfors KK, Micić V, Borovinskaya O, von der Kammer F, Hofmann T, Cornelis G. A critical evaluation of short columns for estimating the attachment efficiency of engineered nanomaterials in natural soils. Environ Sci Nano. 2021;8(6):1801–14.

Publisher's Note